

Generalized Onsager theory for strongly anisometric patchy colloids

H. H. Wensink^{1,*} and E. Trizac²

¹*Laboratoire de Physique des Solides, CNRS UMR 8502,
Université Paris-Sud, 91405 Orsay Cedex, France*

²*Laboratoire de Physique Théorique et Modèles Statistiques,
CNRS UMR 8626, Université Paris-Sud, 91405 Orsay Cedex, France*

(Dated: March 10, 2021)

The implications of soft ‘patchy’ interactions on the orientational disorder-order transition of strongly elongated colloidal rods and flat disks is studied within a simple Onsager-van der Waals density functional theory. The theory provides a generic framework for studying the liquid crystal phase behaviour of highly anisometric cylindrical colloids, which carry a distinct geometrical pattern of repulsive or attractive soft interactions localised on the particle surface. In this paper, we apply our theory to the case of charged rods and disks for which the local electrostatic interactions can be described by a screened-Coulomb potential. We consider infinitely thin rod-like cylinders with a uniform line charge and infinitely thin discotic cylinders with several distinctly different surface charge patterns. Irrespective of the backbone shape, the isotropic-nematic phase diagrams of charged colloids feature a generic destabilization of nematic order, a dramatic narrowing of the biphasic density region and a reentrant phenomenon upon reducing the electrostatic screening. At higher particle density the electrostatic repulsion leads to a complete suppression of nematic order in favour of spatially inhomogeneous liquid crystals.

PACS numbers: 82.70.Dd, 61.30.-v, 64.10.+h

I. INTRODUCTION

Many colloidal dispersions, such as natural clays, and (bio-)macromolecular systems consist of rod- or disk-shaped mesogens whose intrinsic ability to form liquid crystalline order gives rise to unique rheological and optical properties [1]. Despite their abundance in nature, the statistical mechanics of fluids containing anisometric particles in general (and oblate ones in particular) has received far less attention than that of their spherical counterparts. The possibility of a first-order disorder-order transition from an isotropic to a nematic phase was first established theoretically by Onsager [2] in the late 1940s. Although originally devised for rod-like particles in solution, his theory also makes qualitative predictions for plate-like particles based on the central idea that orientation-dependent harshly repulsive interactions alone are responsible for stabilizing nematic order. Subsequent numerical studies have fully established the phase diagram of hard prolate [3–8] and oblate hard cylinders [9–11]. Owing to the simplicity of the interaction potential, hard-body systems constitute an essential benchmark for the study of liquid crystals and their phase stability. Temperature becomes merely an irrelevant scaling factor in the free energy and the phase behaviour is fully determined by the volume fraction occupied by the particles and the aspect ratio. At high volume fraction, additional entropy-driven disorder-order transitions occur where a nematic fluid transforms into positionally ordered phases [12]. Depending on the cylinder aspect

ratio the system may develop a smectic phase, characterized by a one-dimensional periodic modulation along the nematic director, or a columnar phase consisting of columns with a liquid internal structure self-assembled into a two-dimensional crystal lattice. Similar to nematic order, the formation of smectic, columnar or fully crystalline structures is based entirely on entropic grounds [13]; the loss of configurational entropy associated with (partial) crystalline arrangement is more than offset by a simultaneous increase in translational entropy, that is, the average free space each particle can explore becomes larger in the ordered phase.

In most practical cases, however, particle interactions are never truly hard and additional enthalpic contributions impinge on the free energy of the system. Long-ranged interactions usually originate from the presence of surface charges leading to electrostatic repulsions between colloids [14, 15], or from traces of other colloidal components such as non-adsorbing polymers, which act as depletion agents and give rise to effective attractive interactions [16, 17]. Other site-specific interactions may originate from hydrogen-bonding [18] or end-functionalized polymers such as DNA grafted onto the colloid surface [19]. Depending on their nature (repulsive or attractive), interaction range, and topological arrangement on the particle surface, these site-specific directional interactions may greatly affect the self-assembly properties of anisometric particles [20–22]. In this context it is also worth mentioning recent progress in the fabrication of anisometric colloids with ‘patchy’ interactions [23, 24] where the interplay between patchiness and the anisometric backbone shape offers a rich and intriguing repertoire of novel structures [25].

These recent developments suggest the need for a com-

*Electronic address: wensink@lps.u-psud.fr

prehensive theory for lyotropic systems which explicitly accounts for these patchy interactions. The aim of the present paper is to set up such a theory by combining the classic Onsager theory for slender hard bodies, with a mean-field van der Waals treatment for the additional long-ranged interactions [26–30]. Most molecular-field type theories developed to date focus on rod-like mesogens with dispersion interactions represented by an orientation-dependent potential with some radially symmetric spatial variation, akin to a Maier-Saupe form [31, 32]. Here, we shall lay out the framework for the more general case of slender rod and disk-shaped cylinders carrying site interactions with arbitrary integrable form and spatial arrangement. By exploiting the simple second-virial structure of the Onsager reference free energy, we show that these soft patchy interactions, on the mean-field level, give rise to a non-trivial orientation-dependent van der Waals (or molecular field) term which strongly affects the disorder-order transition in the fluid state.

We illustrate its practical use by focusing on isotropic-to-nematic and nematic-to-smectic or columnar phase transitions in systems of charged prolate and discotic colloid in the salt-dominated regime, a subject of considerable research interest given that natural clays consist of strongly charged colloids. The majority of clays are composed of sheet-like mineral colloids [33, 34] but rod-shaped mineral colloids may display similar properties [35–37]. It is still largely unclear how the interplay between particle shape and electrostatics controls the structure and dynamics of clay systems. The fundamental understanding is further complicated by the fact that both the magnitude and sign of the local charge density may vary significantly along the particle surface. For instance, under certain chemical conditions laponite platelets [38] adopt opposite face and rim-charges and the intrinsic patchiness of the electrostatic interactions may lead to unusual liquid behaviour [39]. Incorporating these patchy interactions into a state-of-the-art statistical physical machinery to extract structural information remains a daunting task. Headway can be made by using computer simulation where a number of coarse-grained models for non-isometric charged colloids have been studied over the past decade [40–45].

With the present theory, we aim to set a first step towards linking microscopic patchiness of soft interactions to liquid crystal stability for strongly anisometric colloids. We apply the generalized Onsager theory to the case of charged cylinders interacting through an effective Yukawa potential and demonstrate a generic destabilization and non-monotonic narrowing of the biphasic gap upon reducing the electrostatic screening. The influence of the geometric pattern of the charge patches can be incorporated explicitly by means of a form factor, as shown for disklike colloids. The present calculations, however, merely serve an illustrative purpose and the main goal is to open up viable routes to studying more complicated surface charge architectures of clay nano sheets [46–49] or

anisotropic Janus particles [50, 51]. Moreover, the theory can be further refined by using effective parameters, pertaining to the backbone shape, charge density, screening constant etcetera, in order to enable more quantitative predictions for highly charged anisometric colloids.

Although the Onsager treatment is strictly limited to low to moderate density, it offers possibilities to assess the stability of high-density liquid crystal phases on the level of a simple bifurcation analysis [52]. We show that it is possible to extend the generalized-Onsager form into a full density functional form (e.g. using judicious parametric form for the one-body density) is possible. This holds promise for incorporating soft interactions into more sophisticated hard-body density functionals such as those based on fundamental measure theory [53–55], weighted-density approximations [8], renormalized Onsager theories [30, 56], or cell-theory [3, 7]. The use of reliable non-local reference free energy functionals is expected give a more quantitative account of patchy rods or disks with broken translational symmetry induced by a high particle density, geometric confinement [57] or surfaces [58]. The generalized Onsager theory bears some resemblance to other interaction-site models such PRISM/RISM theories [59, 60] which have been invoked to study the thermodynamic properties of isotropic plate fluids, but have not yet proven capable of treating liquid crystal phases at higher particle densities. The effect of attractive interparticle forces on the bulk phase behaviour of ionic liquid crystals has been scrutinized in Ref. 61 using a mean-field theory of the Gay-Berne potential for ellipsoidal mesogens.

The remainder of this paper is structured as follows. In Section II, we outline the mean-field Onsager theory for soft patchy cylinders with vanishing thickness, while the specific features of the screened Coulomb potential are addressed in section III. The theory will then be applied in Section IV to study the isotropic-nematic phase diagram of charged rod- and disklike cylinders in the strong screening regime. Possible ways to include spatially inhomogeneous liquid crystals into the generalized Onsager treatment are highlighted in Section V. Finally, some concluding remarks are formulated in Section VI.

II. MEAN-FIELD ONSAGER THEORY FOR SOFT PATCHY POTENTIALS

Let us consider a system of N infinitely thin colloidal cylindrical disks or rods with length L and diameter D at positions $\{\mathbf{r}^N\}$ and orientations $\{\Omega^N\}$ in a 3D volume V at temperature T . We assume the particle shape to be maximally anisotropic so that the aspect ratio $L/D \rightarrow \infty$ (infinitely elongated rods) and $L/D \downarrow 0$ (infinitely flat disks). In the fluid state, the particle density $\rho = N/V$ is homogeneous throughout space. Following Onsager’s classical theory [2] we may write the Helmholtz free en-

ergy as follows:

$$\frac{\beta F}{N} \sim \ln \mathcal{V} \rho + \langle \ln 4\pi f(\Omega) \rangle - \frac{\rho}{2} \left\langle \left\langle \int_V d\mathbf{r} \Phi(\mathbf{r}; \Omega_1, \Omega_2) \right\rangle \right\rangle, \quad (1)$$

with $\beta^{-1} = k_B T$ in terms of Boltzmann's constant k_B and \mathcal{V} the total thermal volume of a cylinder, defined from the cube of the de Broglie wavelength, dressed by contributions from the rotational momenta since the kinetic energy not only consists of translational terms. The value of \mathcal{V} will prove immaterial in the subsequent analysis. The brackets denote orientation averages $\langle \cdot \rangle = \int d\Omega f(\Omega) (\cdot)$ and $\langle \langle \cdot \rangle \rangle = \iint d\Omega_1 d\Omega_2 f(\Omega_1) f(\Omega_2) (\cdot)$ in terms of the orientational distribution function (ODF) $f(\Omega)$ which expresses the probability for a cylinder to adopt a solid angle Ω on the 2D unit sphere. The shape of the ODF allows us to distinguish between isotropic order, where $f = 1/4\pi$, and nematic order where f is some peaked function. Particle interactions are incorporated on the second-virial level via a spatial integral over the Mayer function:

$$\Phi(\mathbf{r}; \Omega_1, \Omega_2) = e^{-\beta U(\mathbf{r}; \Omega_1, \Omega_2)} - 1, \quad (2)$$

which depends on the pair potential U between two cylinders with centre-of-mass distance $\mathbf{r} = \mathbf{r}_1 - \mathbf{r}_2$. In our model we shall assume each particle to consist of a cylindrical hard core (HC) with diameter D and height L supplemented with a soft interaction potential U_s describing (effective) long-ranged interaction with neighboring particles. These soft interactions can either be repulsive or attractive and may originate from effective interparticle forces between the colloids under the influence of depletion effects [17], polymers end-grafted onto the colloid surface [62] or electrostatics [14]. The corresponding potential is unlikely to be a simple radially symmetric function but rather emerges from a particular spatial arrangement of interaction sites located on the cylinder surface. In the latter case the soft potential is given by a summation over site-site interactions which are assumed to have a radially symmetric form $u(r)$ [110]

$$U_s(\mathbf{r}; \Omega_1, \Omega_2) = \sum_{l,m} u(|\mathbf{r} + \mathbf{s}_l(\Omega_1) - \mathbf{s}_m(\Omega_2)|), \quad (3)$$

where \mathbf{s}_i denotes the distance vector between site l located on the surface of cylinder 1 and the centre-of-mass \mathbf{r}_1 . The total pair potential thus reads:

$$U(\mathbf{r}; \Omega_1, \Omega_2) = \begin{cases} \infty & \text{if hard cores overlap} \\ U_s(\mathbf{r}; \Omega_1, \Omega_2) & \text{otherwise.} \end{cases} \quad (4)$$

For hard cylinders ($U_s = 0$), the spatial integral over the Mayer function yields the excluded volume between two cylinders at fixed orientations. In the limit of maximal cylinder anisotropy, one obtains [2]:

$$v_{\text{excl}}(\gamma) = - \int_V d\mathbf{r} \Phi_{HC}(\mathbf{r}; \Omega_1, \Omega_2) = v_0 |\sin \gamma|, \quad (5)$$

with $v_0 = 2L^2 D$ for needles ($L/D \rightarrow \infty$) and $v_0 = \pi D^3/2$ for disks ($L/D \downarrow 0$). $\gamma(\Omega_1, \Omega_2)$ denotes the enclosed angle between the normal vectors of two cylinders. The total free energy of the fluid can be compactly written as:

$$\frac{\beta F}{N} \sim \ln \mathcal{V} \rho + \langle \ln 4\pi f(\Omega) \rangle + \frac{\rho}{2} \langle \langle v_{\text{excl}}(\gamma) \rangle \rangle + \frac{\rho}{2} \left\langle \left\langle \int_{\mathbf{r} \notin v_{\text{excl}}} d\mathbf{r} \left(1 - e^{-\beta U_s(\mathbf{r}; \Omega_1, \Omega_2)} \right) \right\rangle \right\rangle. \quad (6)$$

The spatial integral in the final term runs over the space complementary to the finite excluded volume manifold formed by the hard cores of two cylinders at fixed orientations. The last term can be interpreted as an *effective* excluded volume but a direct calculation of this quantity poses some serious technical difficulties [63]. A more tractable expression can be obtained by adopting a mean-field form which can be obtained by taking the limit $\beta U_s \ll 1$ in the second-virial term. Eq. (6) can then be recast into a form resembling a generalised van der Waals free energy:

$$\frac{\beta F}{N} \sim \ln \mathcal{V} \rho + \langle \ln 4\pi f(\Omega) \rangle + \frac{\rho}{2} \langle \langle v_{\text{excl}}(\gamma) \rangle \rangle + \frac{\beta \rho}{2} (a_0 - \langle \langle a_1(\Omega_1, \Omega_2) \rangle \rangle), \quad (7)$$

where the contributions a_0 and a_1 can be identified as van der Waals constants emerging from spatial averages of the soft potential. The non-trivial one, a_1 , runs over the excluded volume manifold of the cylinders:

$$a_1(\Omega_1, \Omega_2) = \int_{\mathbf{r} \in v_{\text{excl}}} d\mathbf{r} U_s(\mathbf{r}; \Omega_1, \Omega_2), \quad (8)$$

whereas a_0 represents an integration over the entire spatial volume V :

$$a_0 = \int_V d\mathbf{r} U_s(\mathbf{r}; \Omega_1, \Omega_2) = \sum_{l,m} \int_V d\mathbf{r} u(|\mathbf{r} + \mathbf{s}_l(\Omega_1) - \mathbf{s}_m(\Omega_2)|). \quad (9)$$

Introducing a linear coordinate transformation $\mathbf{y} \rightarrow \mathbf{r} + \mathbf{s}_l(\Omega_1) - \mathbf{s}_m(\Omega_2)$ (with Jacobian unity) yields a trivial constant:

$$a_0 = \sum_{l,m} \int_V d\mathbf{y} u(|\mathbf{y}|) = 4\pi \int_0^\infty dr r^2 u(r) = \text{cst}, \quad (10)$$

independent of the mutual cylinder orientation. In arriving at Eq. (10), we have tacitly assumed that the spatial integral over the soft part of the pair potential is bounded. For this to be true, the 3D Fourier transform (FT) of the site potential must exist:

$$\hat{u}(q) = 4\pi \int_0^\infty dr r^2 \frac{\sin qr}{qr} u(r). \quad (11)$$

This requires that the potential be less singular than $1/r^3$ in the limit $r \downarrow 0$ and decay sufficiently fast to zero as

$r \rightarrow \infty$. Steep repulsive potentials such as those associated with dipolar interactions, $u \sim 1/r^3$, or van der Waals dispersion forces, $u \sim -1/r^6$ [64], do not qualify and our treatment is aimed at potentials such as the screened-Coulomb (Yukawa) potential [14] or various bounded potentials such as Gaussian [65, 66], square-well [67, 68] or linear ramp potentials which routinely arise from free-volume type theories for depletion interactions [17] or as effective potentials for end-grafted polymers [62]. We remark that the free energy Eq. (7) represents a hybrid between the second-virial approach, which is valid at low particle densities, and the mean-field approximation, accurate at high particle density. For charged cylinders it will be shown that the theory represent a simplified alternative to a more formal variational hard-core Poisson-Boltzmann theory for anisometric hard cores developed in Ref. 69 and a coarse-grained density functional theory for Yukawa fluids in Ref. 70.

We shall now proceed with analysing the non-trivial van-der-Waals contribution Eq. (8). In view of the existing FT it is expedient to recast the spatial integral in Eq. (7) in reciprocal space. The analysis is further facilitated by using the linear transform introduced right after Eq. (9). After some rearranging the angle-dependent van der Waals term, Eq. (8) can be factorized in Fourier space in the following way:

$$a_1(\Omega_1, \Omega_2) = \frac{1}{(2\pi)^3} \int d\mathbf{q} \hat{u}(q) W(\mathbf{q}; \Omega_1) W(-\mathbf{q}; \Omega_2) \times \hat{v}_{\text{excl}}(\mathbf{q}; \Omega_1, \Omega_2), \quad (12)$$

in terms of the FT of the excluded volume manifold of two cylinders (calculated in the Appendix):

$$\hat{v}_{\text{excl}}(\mathbf{q}; \Omega_1, \Omega_2) = \int_{\mathbf{r} \in v_{\text{excl}}} d\mathbf{r} e^{i\mathbf{q} \cdot \mathbf{r}} = v_0 |\sin \gamma| \mathcal{F}(\mathbf{q}; \Omega_1, \Omega_2), \quad (13)$$

where the expressions for \mathcal{F} are given explicitly in the Appendix. The contribution W pertains to a FT of the spatial resolution of the interaction sites according to:

$$W(\mathbf{q}; \Omega_\alpha) = \sum_l e^{i\mathbf{q} \cdot \mathbf{s}_l(\Omega_\alpha)}, \quad \alpha = 1, 2 \quad (14)$$

which may be interpreted as a *form factor* reflecting the internal structure of the interaction sites on the particle surface. The simplest case, a point segment located at the centre-of-mass thus corresponds to $\mathbf{s}_1 = \mathbf{s}_2 = \mathbf{0}$ so that $W = 1$. More complicated configurations shall be considered in the following Section.

Next, the equilibrium form of the ODF is obtained by a formal minimization of Eq. (7) :

$$\frac{\delta}{\delta f} \left(\frac{\beta F}{N} - \lambda \langle 1 \rangle \right) = 0, \quad (15)$$

where the Lagrange parameter λ ensures the ODF to be normalised on the unit sphere. The associated self-

consistency equation for the ODF reads:

$$f(\Omega_1) = \mathcal{Z}^{-1} \exp[-\rho \langle (v_{\text{excl}}(\Omega_1, \Omega_2) - \beta a_1(\Omega_1, \Omega_2)) \rangle_2], \quad (16)$$

with normalisation constant $\mathcal{Z} = \langle \exp[\cdot] \rangle_1$ and $\langle \cdot \rangle_j = \int d\Omega_j f(\Omega_j) \langle \cdot \rangle$ a one-body average over the angular set Ω_j at fixed $\Omega_{i \neq j}$. It is easy to see that the isotropic solution $f = \text{cst}$, i.e., all orientations being equally probable, is a trivial solution of the stationarity condition. Beyond a critical particle density non-trivial nematic solutions will appear which can be obtained by numerically solving Eq. (16) [71]. Once the equilibrium ODF is established for a given density phase equilibria between isotropic and nematic states can be investigated by equating the pressure P and chemical potential μ in both states. These are obtained by standard thermodynamic derivatives of the free energy Eq. (7):

$$\begin{aligned} \beta P &= \rho + \frac{\rho^2}{2} \langle \langle v_{\text{excl}}(\Omega_1, \Omega_2) + \beta a_0 - \beta a_1(\Omega_1, \Omega_2) \rangle \rangle \\ \beta \mu &= \ln \rho \mathcal{V} + \langle \ln 4\pi f(\Omega) \rangle \\ &\quad + \rho \langle \langle v_{\text{excl}}(\Omega_1, \Omega_2) + \beta a_0 - \beta a_1(\Omega_1, \Omega_2) \rangle \rangle. \end{aligned} \quad (17)$$

The thermodynamic properties of the isotropic-nematic transition can be calculated by numerically solving these coexistence equations in combination with Eq. (16), the stationarity condition for the ODF. Collective orientation order of cylinders with orientation unit vector $\hat{\mathbf{u}}$ order can be probed by introducing a common nematic director $\hat{\mathbf{n}}$ and defining nematic order parameters such as:

$$S_n = \langle \mathcal{P}_n(\hat{\mathbf{u}} \cdot \hat{\mathbf{n}}) \rangle, \quad (18)$$

where \mathcal{P}_n represents a n th-order Legendre polynomial (e.g. $\mathcal{P}_2(x) = (3x^2 - 1)/2$). Odd contributions of S_n are strictly zero for non-polar phases and S_2 is routinely used to discriminate isotropic order ($S_2 = 0$) from uniaxial nematic order $S_2 \neq 0$.

III. GENERALIZED SCREENED-COULOMB POTENTIAL FOR CYLINDERS

In this section, we shall analyze a simple model for charged anisotropic colloidal particles. Let us consider two disk-shaped macro-ions with total surface charge Z in a electrolyte solution with ionic strength determined by the counter ions and additional co- and counter ions due to added salt. Formally, the electrostatic potential around the charged surface of a macro-ion in an ionic solution with a given ionic strength can be reasonably obtained from the non-linear Poisson-Boltzmann (PB) equation [14]. This theory neglects any correlations between micro-ions and assumes the solvent to be treated as a continuous medium with a given dielectric constant. In the Debye-Hückel approximation, valid if the electrostatic potential at the macro-ion surface is smaller than the thermal energy, the PB equation can be linearized and the electrostatic interaction between

two point macro-ions with equal charge $\pm Ze$ in a dielectric solvent with relative permittivity ε_r is given by the screened-Coulomb or Yukawa form:

$$\beta u_0(r) = Z^2 \lambda_B \frac{e^{-\kappa r}}{r}, \quad (19)$$

with ε_0 the dielectric permittivity in vacuum, r the distance between the macro-ions, $\lambda_B = \beta e^2 / 4\pi \varepsilon_0 \varepsilon_r$ the Bjerrum length ($\lambda_B = 0.7 \text{ nm}$ for water at $T = 298 \text{ K}$) and κ^{-1} the Debye screening length which measures the extent of the electric double layer. In the limit of strong electrostatic screening, the screening factor is proportional to $\kappa = (8\pi \lambda_B n_0)^{1/2}$ with n_0 the concentration of added 1:1 electrolyte. In general, for highly charged colloids, non-linear effects of the PB equation can be accounted for by invoking a cell approximation [72, 73] which assumes a fully crystalline structure where each particle is compartmentalized in Wigner-Seitz cells or a so-called Jellium model [74] where a tagged particle is exposed to a structureless background made up by its neighboring particles. Both methods allow for a solution of the full non-linear PB equation for an isolated colloidal with the effect of the surrounding charged particles subsumed into a suitable boundary condition. This procedure yields so-called *effective* values for the charge $Z_{\text{eff}} < Z$ and Debye screening constant κ_{eff} which can be used to achieve accurate predictions for the thermodynamic properties (e.g. osmotic pressure) of fluids of highly charged spheres [75]. We will briefly touch upon these effective parameters in paragraph C of this section. We reiterate that we focus here on the high-salt regime where use of the linearized form Eq. (19) combined with effective electrostatic parameters is deemed appropriate. The low-screening regime requires a lot more care due the fact that the effective interaction becomes inherently dependent on the macroion density. As a consequence, the free energy contains non-trivial volume terms which may have important implications for the fluid phase behaviour [76–78].

The FT of the Yukawa potential is given by a simple Lorentzian:

$$\hat{u}(q) = Z^2 \lambda_B \frac{4\pi}{q^2 + \kappa^2}. \quad (20)$$

The spatial average over Eq. (19) yields for a_0 :

$$\beta a_0 = 4\pi Z^2 \lambda_B \kappa^{-2}. \quad (21)$$

We may generalize the screened-Coulomb potential for a cylindrical object by imposing that the total effective electrostatic potential be given by a sum over n identical Yukawa sites located on the cylinder surface. As per Eq. (3) the pair potential is given by:

$$\beta U_s = \frac{Z^2 \lambda_B}{n^2} \sum_{i,j < n} \frac{\exp[-\kappa |\mathbf{r} + \mathbf{s}_i(\Omega_1) - \mathbf{s}_j(\Omega_2)|]}{|\mathbf{r} + \mathbf{s}_i(\Omega_1) - \mathbf{s}_j(\Omega_2)|}. \quad (22)$$

We note that the generalized form is only adequate for non-isometric hard cores with a vanishing internal volume [41]. Such objects can be obtained, e.g., by taking

a cylindrical object with an extreme aspect ratio. In the next paragraphs, we shall analyze the expression above for infinitely elongated rods ($D/L \downarrow 0$) and subsequently for flat cylindrical disks ($L/D \downarrow 0$).

A. Needle limit

In case of infinitely slender charged rods, we assume a continuous distribution of sites located along the normal unit vector $\hat{\mathbf{u}}$ running through the centre-of-mass of the cylinder. The result is a double integration along the one-dimensional contours of the rod pair. Defining a dimensionless contour parameter ℓ_i , so that $\mathbf{s}(\Omega_\alpha) = \ell_\alpha L \hat{\mathbf{u}}_\alpha$ the generalized screened-Coulomb potential between rodlike particles can be written as:

$$\beta U_s = Z^2 \lambda_B \int_{-\frac{1}{2}}^{\frac{1}{2}} d\ell_1 \int_{-\frac{1}{2}}^{\frac{1}{2}} d\ell_2 \frac{\exp[-\kappa |\mathbf{r} + L(\ell_1 \hat{\mathbf{u}}_1 - \ell_2 \hat{\mathbf{u}}_2)|]}{|\mathbf{r} + L(\ell_1 \hat{\mathbf{u}}_1 - \ell_2 \hat{\mathbf{u}}_2)|}. \quad (23)$$

A closed-form solution of the electrostatic rod potential was reported in Ref. 79 and a generalized DLVO form for rodlike macro-ions has been analyzed in Refs. 80, 81. A tractable form for the electrostatic potential between infinitely stretched linear charges was used by Onsager in his seminal paper [2, 82] based on a limiting form for $\kappa L \rightarrow \infty$ [83].

Since our focus is on a simple van der Waals description for uniform fluids ($\rho = \text{cst}$), the compound form of Eq. (23) naturally deconvolutes into a spherically symmetric kernel $\hat{u}(q)$ and form factor W (cf. Eq. (12)). It is obvious that such a factorization becomes much more complicated in the columnar, smectic or crystalline states where inhomogeneities in the density field are intricately coupled to the distance-variation of the electrostatic potential. This we shall see in more detail in Section V. We may specify the form factor by considering a linear array of interaction sites [84]. In the continuum limit, Eq. (14) becomes:

$$\begin{aligned} W_{\text{needle}}(\mathbf{q}; \Omega_\alpha) &= \int_{-\frac{1}{2}}^{\frac{1}{2}} d\ell_\alpha e^{-iL\mathbf{q} \cdot \hat{\mathbf{u}}_\alpha} \\ &= j_0 \left(\frac{L}{2} \mathbf{q} \cdot \hat{\mathbf{u}}_\alpha \right), \quad \alpha = 1, 2 \end{aligned} \quad (24)$$

with $j_0(x) = \sin x/x$ a spherical Bessel function. With this the orientation-dependent van der Waals constant Eq. (12) for rods is completely specified. The remaining 3D integration over reciprocal space must be carried out numerically for every orientation. Note that an evaluation in real space would confront us with a five-fold numerical integration since Eq. (23) cannot be solved analytically. To facilitate the integration over q -space, we adopt a particle-based frame $\{\hat{\mathbf{u}}_1, \hat{\mathbf{u}}_2, \hat{\mathbf{v}}\}$ introduced in the Appendix. This allows us to reexpress the dot products in terms of the angle γ between the main axis of the

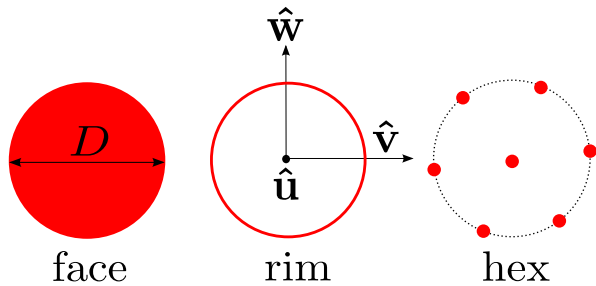


FIG. 1: Sketch of three possible surface charge patterns for infinitely thin disks. From left to right: uniform distribution over the circular face with diameter D (“face”), one-dimensional distribution along the outermost circular contour (“rim”) and a discrete hexagonal arrangement (“hex”).

rod pair via:

$$\begin{aligned} L\mathbf{q} \cdot \hat{\mathbf{u}}_1 &= q_1 + q_2 \cos \gamma \\ L\mathbf{q} \cdot \hat{\mathbf{u}}_2 &= q_1 \cos \gamma + q_2 \\ D\mathbf{q} \cdot \hat{\mathbf{v}} &= q_3, \end{aligned} \quad (25)$$

and $\int d\mathbf{q} = (L^2 D)^{-1} |\sin \gamma| \prod_{i \leq 3} \int_{-\infty}^{\infty} dq_i$. The integration over q_3 can be carried out analytically and the remaining expression can be simplified by taking the leading order contribution in the needle limit $x = D/L \ll 1$. The mean-field contribution $a_1(\gamma)$ for strongly elongated charged rods then reads in normalized form:

$$\begin{aligned} \frac{a_1(\gamma)}{a_0} &= \frac{1}{4\pi^2} (1 - e^{-\kappa D}) \sin^2 \gamma \int_{-\infty}^{\infty} dq_1 \int_{-\infty}^{\infty} dq_2 \\ &\quad \times j_0^2(L\mathbf{q} \cdot \hat{\mathbf{u}}_1) j_0^2(L\mathbf{q} \cdot \hat{\mathbf{u}}_2). \end{aligned} \quad (26)$$

Recalling that $a_0 \propto \kappa^{-2}$ one can infer that a_1 vanishes in the limit of infinite screening $\kappa D \rightarrow \infty$ and diverges in the Coulomb limit ($\kappa D \downarrow 0$) [85] as one would intuitively expect.

B. Flat disk limit

We now turn to the case of infinitely thin disks. As for the needles, we assume a continuous charge distribution along circular surface of the disk, which is most conveniently parameterized by invoking the particle-based coordinate frame (see Appendix) so that:

$$\mathbf{s}(\Omega_\alpha) = \frac{D}{2} r_\alpha (\hat{\mathbf{v}} \cos \xi_\alpha + \hat{\mathbf{w}}_\alpha \sin \xi_\alpha), \quad (27)$$

where $0 \leq r_\alpha \leq 1$ and $0 \leq \xi_\alpha \leq 2\pi$. The electrostatic potential between two flat disks at fixed orientations is represented by a four-fold integral:

$$\begin{aligned} \beta U_s &= Z^2 \lambda_B \frac{1}{\pi^2} \prod_{\alpha=1,2} \int_0^1 dr_\alpha r_\alpha \int_0^{2\pi} d\xi_\alpha \\ &\quad \times \frac{\exp[-\kappa |\mathbf{r} + \mathbf{s}(\Omega_1) - \mathbf{s}(\Omega_2)|]}{|\mathbf{r} + \mathbf{s}(\Omega_1) - \mathbf{s}(\Omega_2)|}. \end{aligned} \quad (28)$$

The form factor associated with a discotic arrangement of surface charges is given by the cosine transform of Eq. (27):

$$\begin{aligned} W_{\text{face}}(\mathbf{q}; \Omega_\alpha) &= \frac{1}{\pi} \int_0^1 dr_\alpha r_\alpha \int_0^{2\pi} d\xi_\alpha \cos(\mathbf{q} \cdot \mathbf{s}(\Omega_\alpha)) \\ &= 2J_1(\tilde{q}_\alpha)/\tilde{q}_\alpha, \end{aligned} \quad (29)$$

with $J_n(x)$ a Bessel function of the first kind and $\tilde{q}_\alpha = [(\frac{D}{2} \mathbf{q} \cdot \hat{\mathbf{w}}_\alpha)^2 + (\frac{D}{2} \mathbf{q} \cdot \hat{\mathbf{v}})^2]^{1/2}$. We may also consider the situation where the charges are distributed along the circular rim of the disk (Fig. 1). The corresponding form factor simply follows from Eq. (27) and Eq. (28) by setting $r_\alpha = 1$ and integrating over the remaining angular part:

$$\begin{aligned} W_{\text{rim}}(\mathbf{q}; \Omega_\alpha) &= \frac{1}{2\pi} \int_0^{2\pi} d\xi_\alpha \cos\left(\frac{D}{2} (\hat{\mathbf{v}} \cos \xi_\alpha + \hat{\mathbf{w}}_\alpha \sin \xi_\alpha)\right) \\ &= J_0(\tilde{q}_\alpha). \end{aligned} \quad (30)$$

Alternatively, we may consider a discrete hexagonal arrangement of surface charges (see Fig. 1), in which case the form factor becomes:

$$\begin{aligned} W_{\text{hex}}(\mathbf{q}; \Omega_\alpha) &= \frac{1}{7} \left(1 + \cos(D\mathbf{q} \cdot \hat{\mathbf{v}}) + 2 \cos\left(\frac{D}{2} \mathbf{q} \cdot \hat{\mathbf{v}}\right) \right. \\ &\quad \left. \times \cos\left(\frac{D\sqrt{3}}{2} \mathbf{q} \cdot \hat{\mathbf{w}}_\alpha\right) + (\hat{\mathbf{v}} \leftrightarrow \hat{\mathbf{w}}_\alpha) \right) \end{aligned} \quad (31)$$

The last term ensures that the form factor remains invariant with respect to a rotation in the $\hat{\mathbf{v}}, \hat{\mathbf{w}}_\alpha$ plane so that W_{hex} attains the same symmetry as the expressions for the “face” and “rim” patterns. The additional angular correlations naturally arise from the discrete nature of the hexagonal pattern. In view of the fluid phases considered here, they are deemed of negligible importance. We remark that all form factors approach the radially symmetric limit ($W = 1$) in the macroscopic limit $q \downarrow 0$. Similar to the needle case the FT definition of the van der Waals contribution Eq. (12) reduces the dimensionality of the problem to a straightforward integration over 3D q -space whereas the real-space route would confront us with an intractable seven-fold integration. Analogous to Eq. (25), the integration over reciprocal space can be parameterized using the particle-based frame for disks (see Appendix): $D\mathbf{q} \cdot \hat{\mathbf{w}}_1 = q_1 + q_2 \cos \gamma$, $D\mathbf{q} \cdot \hat{\mathbf{w}}_2 = q_1 \cos \gamma + q_2$, and $D\mathbf{q} \cdot \hat{\mathbf{v}} = q_3$ so that a_1 depends only on enclosed angle γ between the normal vectors of the disks as should be the case for apolar uniaxial cylinders.

Judging from Eq. (16), it is evident that a_1 can be identified with an aligning potential of mean force $V_{\text{mf}}(\Omega)$, reflecting the average potential incurred by the soft potential of all the surrounding cylinders. This potential is inherently density-dependent and reads:

$$V_{\text{mf}}(\Omega) = -\rho \int d\Omega' a_1(\gamma(\Omega, \Omega')) f(\Omega'), \quad (32)$$

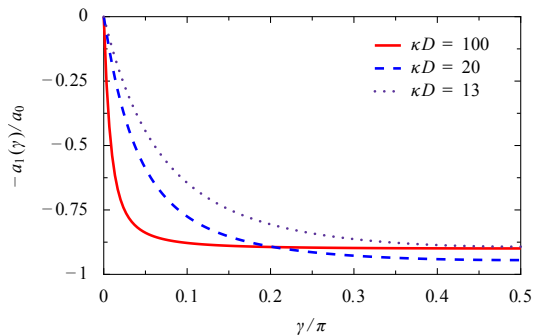


FIG. 2: Aligning potential of mean force (in dimensionless units) for infinitely thin Yukawa disks with a homogeneous distribution of screened charges covering the circular surface of the disk. Shown are curves for different ionic strengths κD . Near-parallel disk orientations ($\gamma \sim 0$) are strongly disfavored.

where the ODF f depends implicitly on ρ . Its angular dependence generally disfavours parallel orientations, as illustrated in Fig. 2 for the case of disks with a continuous distribution of Yukawa sites (“face”). Similar monotonically decreasing functions are obtained for rods with the screening constant κD governing the typical range of the potential. We reiterate that $a_1(\gamma)$ represents a distance-averaged orientational mean-field potential which is only applicable in the context of uniform isotropic or nematic fluids. On the other hand, the spatially resolved electrostatic potential for charged disks bears an intricate coupling between the mutual orientation and centre-of-mass separation distance of the disk pair such that, at least in the far-field limit, coaxial pair configurations are favored over planar ones (see Eq. (33) in Section III-C) [41, 86]. At high particle density, the interplay between near-field steric and far-field electrostatic forces may drive the formation of liquid crystalline structures with unusual positional and orientational microstructure [42, 45], thereby significantly affecting the stability of smectic and columnar order as we shall see in Section V.

C. Second-virial coefficient for highly charged disks

In this Section, we shall look at an alternative route towards incorporating electrostatic interactions into the Onsager density functional theory for the case of highly charged discotic colloids. The objective is to make an estimate of the total second-virial coefficient of a charged disk. The orientational dependence of this quantity gives us an idea of the effective shape (anisometry) of a charged discotic object and its propensity to form orientationally ordered phases at various screening conditions [63]. To circumvent the computational burden associated with a spatial integration of the Mayer function for segment potentials, we shall consider a tractable form for the electrostatic potential that can be obtained from non-linear

(as well as linearized) Poisson-Boltzmann theory. In the *far-field* limit, the latter potential for anisotropic colloids can be recast into the following form [41, 86, 87]:

$$U_s(\mathbf{r}; \Omega_1, \Omega_2) = Z_{\text{eff}}^2 \lambda_B \xi(\kappa D, \vartheta_1) \xi(\kappa D, \vartheta_2) \frac{e^{-\kappa r}}{r}. \quad (33)$$

The anisotropy function $\xi(\kappa D, \vartheta)$ depends on the screening parameter κ and the angle ϑ between the centre-of-mass distance vector $\hat{\mathbf{r}}$ and disk normal $\hat{\mathbf{u}}$ such that $\cos \vartheta = \hat{\mathbf{r}} \cdot \hat{\mathbf{u}}$. Generally ξ increases with ϑ and reaches a maximum at $\vartheta = \pi/2$. Eq. (33) tells us that the orientation-dependence of the electrostatic potential is retained in the far-field limit, and that stacked pair configurations are energetically favored over co-planar ones, irrespective of the centre-of-mass separation distance r .

For highly charged colloidal disks, the strong coupling between the macro- and micro-ion charges leads to non-linear effects (such as counterion condensation) which can be quantified from the non-linear PB equation. The non-linearities can be taken into account by replacing the bare charge by an *effective* renormalized charge Z_{eff} . Its saturation value depends on the screening parameter and can be estimated as $Z_{\text{eff}}^{\text{sat}} \lambda_B / D \approx 0.5 \kappa D + 1.12$ [87]. An approximate form for the anisotropy function is given by [41]:

$$\xi(\kappa D, \vartheta) = 2 \frac{I_1\left(\frac{\kappa D}{2} \sin \vartheta\right)}{\frac{\kappa D}{2} \sin \vartheta}, \quad (34)$$

with $\sin \vartheta = (1 - (\hat{\mathbf{r}} \cdot \hat{\mathbf{u}})^2)^{1/2}$ and $I_1(x)$ a modified Bessel function of the first kind. Improved expressions can be found in [87].

Within Onsager’s original second-virial approximation, the excess free energy is proportional to the second-virial coefficient B_2 embodied by the last two terms of Eq. (6). The excess free energy can thus be compactly written as:

$$\frac{\beta F_{\text{ex}}}{N} = -\frac{\rho}{2} \langle \langle \beta_1(\Omega_1, \Omega_2) \rangle \rangle = \rho B_2, \quad (35)$$

where the cluster integral β_1 is given by a spatial integral of the Mayer function Eq. (2). For the electrostatic part we need to integrate over the space complementary to the excluded volume between two infinitely thin disks for which we may invoke the parameterization Eq. (52) proposed in the Appendix. The cluster integral then becomes:

$$\beta_1(\gamma) = -v_{\text{excl}}(\gamma) + \left(\int_V d\mathbf{r} - \prod_{i=1,3} \int_{-1}^1 dt_i J_{cc} \right) \Phi(t_i; \gamma), \quad (36)$$

with $J_{cc} = \frac{D^3}{8} |\sin \gamma| [(1 - t_1^2)^{1/2} + (1 - t_2^2)^{1/2}]$ the Jacobian associated with the transformation from the Cartesian lab frame to the particle frame and Φ the Mayer function given by Eq. (2). Since both volume integrals

are defined within the latter frame, the orientation degrees of freedom naturally condense into a single angle γ between the disk normals. Comparing Eq. (36) to the van der Waals form for patchy cylinders Eq. (12) we see that both expressions involve a 3D integration in Fourier or real space which can be numerically resolved without difficulty.

IV. RESULTS FOR THE ISOTROPIC-NEMATIC TRANSITION

We now turn to the isotropic-nematic phase diagram for charged cylinders in the extreme aspect ratio limit. Let us first concentrate on the case of infinitely elongated rodlike cylinders with $L/D \rightarrow \infty$. The physical quantities of interest are the dimensionless concentration $c = \rho L^2 D$, the charge Z , and the amplitude of the screened Coulomb potential. It is customary to define a linear charge density σ indicating the number of elementary charges per unit length so that the total rod charge $Z = \sigma L$ leads to a dimensionless amplitude $\sigma^2 D \lambda_B$. If we take a typical rod diameter of $D \sim 10 \text{ nm}$ the Yukawa amplitudes in Fig. 3 corresponds to a linear charge density σ of several elementary charges per nm . Furthermore we consider the case of excess salt so that the screening constant κ does not depend on the colloid concentration. The phase diagram in Fig. 3 features a dramatic narrowing of the biphasic gap at lower ionic strength and a significant weakening of nematic order of the coexisting nematic phase. The negative sign of S_4 reflects an increased propensity for the rods to adopt perpendicular pair configurations at low screening so as to minimize the overlap of their electric double layers. This is a manifestation of the so-called “electrostatic twist” for line charges which has been quantified in detail in Ref. 82. The rapid variation of the binodal densities at low ionic strength reveals a marked re-entrant phase separation effect. A homogeneous isotropic sample at fixed particle density (say $c \sim 5.3$) undergoes a sequence of phase transformations upon increasing the ionic strength. First, the system exhibits isotropic-nematic phase coexistence with a weak density contrast. Second, the sample reverts to a homogeneous isotropic state before re-entering into a phase-separation with a strong density difference between the coexisting phases. The isotropic-nematic transition disappears below a critical screening constant which is roughly independent of the line charge. The narrowing of the phase gap and upward shift of the transition density as the strength of the electrostatic interaction potential increases are both generic features of charged anisometric colloids, consistent with predictions from previous mean-field theories for rods in the Coulomb limit [85], and at finite screening [82].

We remark that most colloidal systems consist of highly charged colloidal objects and that non-linear effects arising from the PB equation must be taken into account. As alluded to before, this can be done by re-

taining the linearized Debye-Hückel form and using a “dressed” renormalized line charge σ_{eff} which depends, in general, on the macro-ion density, shape and salt concentration. Despite the highly non-trivial relation between these quantities, it is possible to derive simple analytical estimates for the saturation value, such that, for strongly elongated cylinders one can write $\sigma_{\text{eff}}^{\text{sat}} \lambda_B \sim \kappa D$ [88]. However, within the current scheme no stable nematic phase is found when simply replacing σ by σ_{eff} in case of strong screening since $(\sigma_{\text{eff}}^{\text{sat}})^2 \lambda_B D \gg 1$ and the isotropic-nematic transition will be completely obstructed by the denematizing mean-field potential $a_1(\gamma)$. Two remarks are in order. First, the absence of a thermodynamically stable nematic phase could be a spurious result of the present theoretical set-up that may be remedied, at least in part, by devising a more refined free energy by carrying over part of the harshly repulsive near-field electrostatic potential into the second virial coefficient e.g. by introducing an effective diameter $D_{\text{eff}} > D$. This opens up ways to designing optimized schemes that combine an effective particle shape with an appropriately rescaled aligning background potential capturing the far-field electrostatics at high particle density. These ideas have been pursued in detail in Refs. 69, 70 and Ref. 63 and shall not be further discussed here. Second, the complete destabilization of spatially homogeneous orientational order may hint at the presence of more complicated types of nematic order in systems of highly charged rods. In particular, one could imagine the antagonistic effect of short-ranged aligning forces (due to the rod excluded-volume) and long-ranged dealigning ones (embodied in the mean-field potential a_1) to facilitate the formation of nematic phases with strongly inhomogeneous, e.g., cubic, biaxial or periodically modulated director fields [89]. The occurrence of these complex textures remain to be confirmed by experiments or large scale computer simulations of charged rods in the strong coupling limit.

Let us now turn to the case of charged disks. The isotropic-nematic phase diagram emerging from the Onsager-van der Waals theory for the various charge patterns depicted in Fig. 1 is shown in Fig. 4. Similar to the case of rods we observe a marked weakening of nematic order and a narrowing of the biphasic gap. The overall shape of the binodals does not depend too sensitively on the amplitude provided that $Z^2 \lambda_B / D \sim \mathcal{O}(10)$ at most. As observed for rods, the isotropic-nematic ceases to exist below a critical ionic strength. This effect is most noticeable for disks with a continuous charge distribution along the face or rim. For disks with a discrete hexagonal charge patterns the window of stable nematic order is somewhat larger in terms of ionic strength. The curvature of the binodals point to a re-entrant phase separation phenomenon is similar to the case of rods in Fig. 3. For highly charged disks, the suppression of nematic order is even more drastic and is borne out from the second-virial free energy Eq. (35) using the orientation-dependent Yukawa potential Eq. (33). No stable isotropic-nematic was found in the experimentally

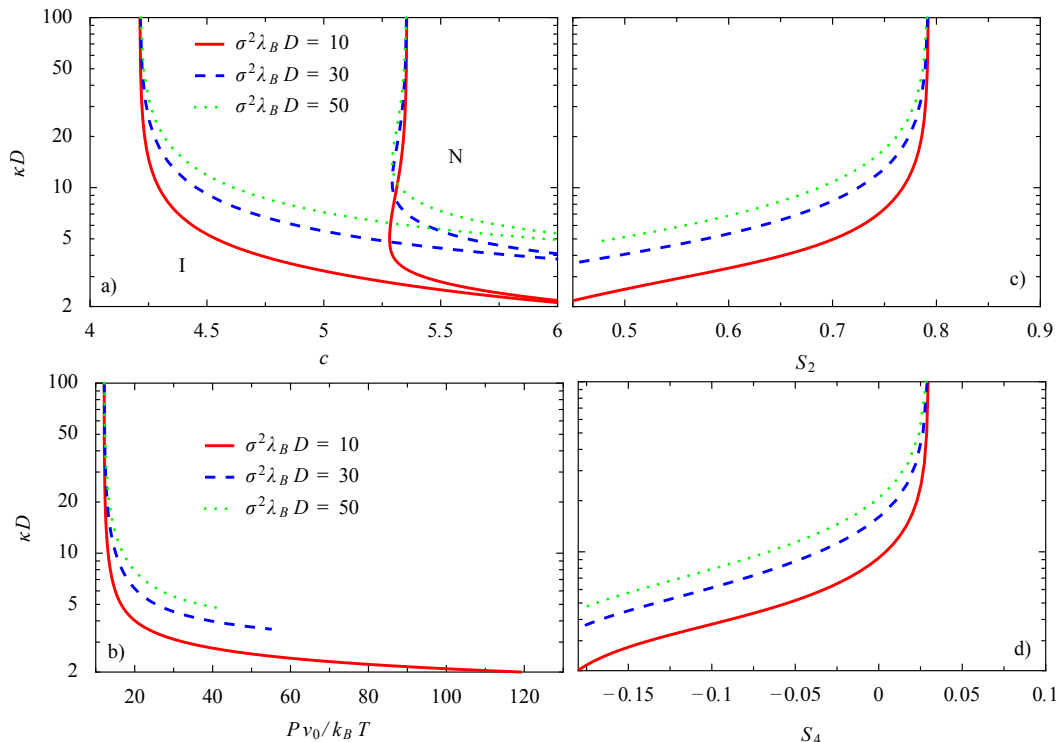


FIG. 3: (a) Isotropic-Nematic phase diagram of charged elongated colloidal rods ($L/D \rightarrow \infty$) for three different values of the Yukawa amplitude $\sigma^2 \lambda_B D$. Plotted are (a) the coexistence densities $c = \rho L^2 D$ versus ionic strength κD . (b) Osmotic pressure P at coexistence. (c-d) Orientational order parameters S_2 and S_4 quantifying the nematic and cubatic order of the nematic phase.

relevant range of disk diameters $35\lambda_B < D < 200\lambda_B$ and densities. The lack of stability of a simple nematic state can be inferred from Fig. 5 illustrating the *effective* excluded volume $-\beta_1$ of a charged disk. Although the volume depends strongly on the ionic strength, its angular variation remains very weak throughout. The effective shape of a highly charged colloidal disk resembles that of a slightly deformed spherical object whose anisotropy is insufficient to generate a thermodynamically stable orientational disorder-order transition. Similar to the case of rods, it is plausible that strongly charged disks exhibit more complicated ordering mechanisms where nematicity is linked to some complex spatial inhomogeneity of the director field as suggested by recent computer simulations [45]. These complex nematic structures call for a more local Onsager free energy that explicitly accounts for the elastic contributions associated with spatial variations of the nematic director [90]. Analogously to the charged rods, the predictive power of the Onsager-van der Waals theory in the strong-coupling regime could be enhanced by combining an effective disk shape with a suitably chosen amplitude for the mean-field aligning potential $a_1(\gamma)$.

V. STABILITY OF LIQUID CRYSTAL PHASES WITH POSITIONAL ORDER

Possible phase transitions to spatially inhomogeneous states with smectic or columnar order can be investigated by recasting the mean-field Onsager into a functional form depending on the one-body density field $\rho(\mathbf{r}, \Omega)$ [90]. Within the framework of classical density-functional theory, the free energy functional needs to be minimised with respect to ρ to yield the unique equilibrium density profile for a given chemical potential, temperature and external potential [91]. In this work, we shall perform a simple stability analysis [92, 93] by assuming a weak periodic density modulation with wave-vector \mathbf{k} and amplitude ε :

$$\rho(\mathbf{r}, \Omega) = \rho_0 f_0(\Omega) + \varepsilon f^*(\Omega) \cos(\mathbf{k} \cdot \mathbf{r}), \quad (37)$$

superimposed onto the one-body density $\rho_0(\mathbf{r}, \Omega) = \rho_0 f_0(\Omega)$ of the spatially homogeneous phase. Beyond a particular value of the bulk density, such a periodic density perturbation will lead to a reduction of the free energy and the homogeneous bulk phase will become marginally unstable. The so-called bifurcation point can be found by inserting Eq. (37) into the density functional and Taylor-expanding up to second order in ε . The resulting bifurcation condition is represented by a linear

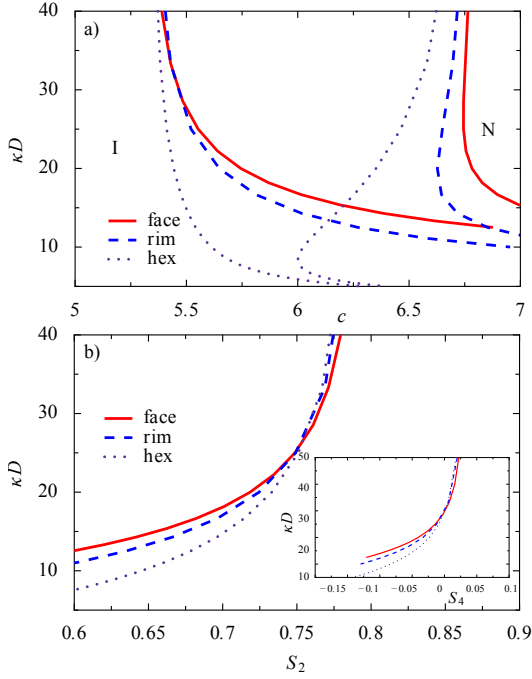


FIG. 4: (a) Isotropic-Nematic binodals for charged disks with charge distributions corresponding to the patterns indicated in Fig. 1. Plotted is the particle concentration $c = \rho D^3$ versus the ionic strength κD . The Yukawa amplitude is $Z^2 \lambda_B / D = 10$. (b) Orientational order parameters of the nematic phase at coexistence.

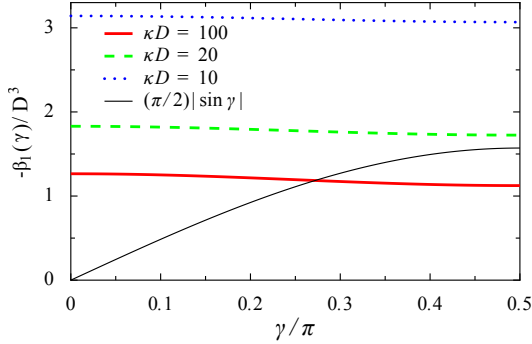


FIG. 5: Effective excluded volume $-\beta_1(\gamma)$ between highly charged disks with diameter $D = 35\lambda_B$ interacting via the orientation-dependent Yukawa potential Eq. (33). The black solid line indicates the bare excluded volume of hard disks.

eigenvalue equation [94]:

$$\int d\Omega_2 f_0(\Omega_1) \hat{\Phi}(\mathbf{k}; \Omega_1, \Omega_2) f^*(\Omega_2) = \frac{1}{\rho_0} f^*(\Omega_1), \quad (38)$$

in terms of the cosine transformed Mayer function:

$$\hat{\Phi}(\mathbf{k}; \Omega_1, \Omega_2) = \int d\mathbf{r} \Phi(\mathbf{r}; \Omega_1, \Omega_2) \cos(\mathbf{k} \cdot \mathbf{r}). \quad (39)$$

The eigenvector $f^*(\Omega)$ probes the angular distribution in the new phase and reflects the intrinsic coupling be-

tween positional and orientational order. A bifurcation to the positionally modulated state occurs at the wave vector \mathbf{k} that generates the smallest eigenvalue $\rho_0 > 0$ of Eq. (38). We reiterate that, in case of a nematic reference state, the ODF $f_0(\Omega)$ depends implicitly on ρ_0 via the self-consistency condition Eq. (16). If both the particle anisotropy and density are sufficiently large, the degree of nematic order is usually very high and fluctuations in the particle orientations are strongly suppressed. Small variations in the ODF are therefore unlikely to contribute to the loss of nematic stability. In those cases it is justified to neglect the translation-rotation coupling and equate $f^*(\Omega) = f_0(\Omega)$. The bifurcation condition then takes the form of a divergence of the static structure factor $S(\mathbf{k})$:

$$S(\mathbf{k})^{-1} = (1 - \rho_0 \langle \langle \hat{\Phi}(\mathbf{k}; \Omega_1, \Omega_2) \rangle \rangle) = 0. \quad (40)$$

By applying the van der Waals approximation outlined in Sec. II, $\hat{\Phi}$ can be expressed as a sum of the hard-core contribution and a part that encodes the effect of the soft potential. Eliminating the angular dependency of the excluded volume \hat{v}_{excl} and form factor W for notational brevity, one arrives at the following expression for the Mayer kernel in Fourier space:

$$\begin{aligned} \hat{\Phi}(\mathbf{k}) &= -\hat{v}_{\text{excl}}(\mathbf{k}) - \hat{u}(k) \\ &+ \frac{1}{(2\pi)^3} \int d\mathbf{q} \hat{u}(q) W(\mathbf{q}) W(-\mathbf{q}) \hat{v}_{\text{excl}}(\mathbf{k} - \mathbf{q}) \end{aligned} \quad (41)$$

The Fourier integral presents a non-trivial mode-coupling term that convolutes the imposed density wave with the modes describing the distance-dependence of the soft interactions. The solution of Eq. (40) (or Eq. (38)) for particles with full orientational degrees of freedom poses a substantial technical task and we shall simplify matters by considering the more tractable case of *parallel* cylinders. Let us equate the particle frame to the lab frame $\{\hat{\mathbf{x}}, \hat{\mathbf{y}}, \hat{\mathbf{z}}\}$ with the cylinder normals pointing along $\hat{\mathbf{z}}$. The excluded volume of two parallel cylinders is again a cylinder with volume $2\pi L D^2$. In Fourier space the excluded volume takes the following form:

$$\hat{v}_{\text{excl}}(\mathbf{q}) = 2\pi L D^2 j_0(L\mathbf{q} \cdot \hat{\mathbf{z}}) \frac{J_1(\sqrt{(D\mathbf{q} \cdot \hat{\mathbf{x}})^2 + (D\mathbf{q} \cdot \hat{\mathbf{y}})^2})}{\frac{1}{2}\sqrt{(D\mathbf{q} \cdot \hat{\mathbf{x}})^2 + (D\mathbf{q} \cdot \hat{\mathbf{y}})^2}}. \quad (42)$$

Due to the parallel orientation it is no longer possible to take the limit of infinite particle anisotropy since the excluded volume vanishes in both limits (similar to setting $\gamma = 0$ in Eq. (5)). Therefore we shall consider the case $D/L \ll x$ (rods) and $L/D \ll x$ (disks) with x a small but finite number and use the volume fraction $\phi = (\pi/4) L D^2 \rho_0$ as a convenient measure for the particle concentration.

We may probe instabilities pertaining to smectic order by identifying $\mathbf{k} = k_S \{0, 0, 1\}$, a one-dimensional periodic modulation along the nematic director. Hexagonal columnar order can be parametrized by a linear superposition of three modulations with wave-vectors $\mathbf{k}_1 =$

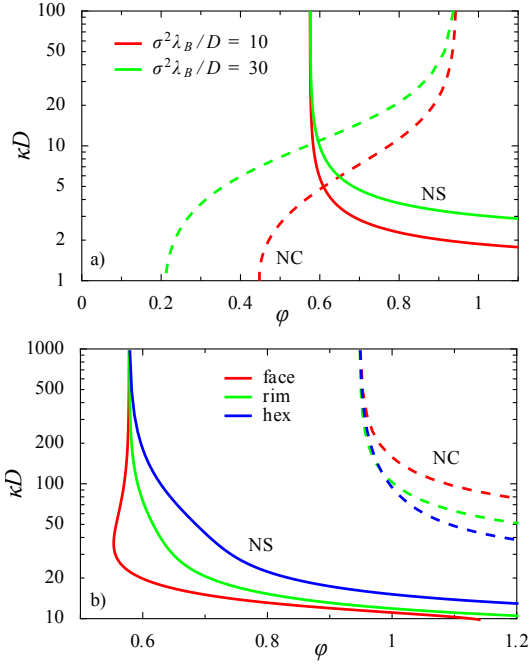


FIG. 6: (a) Variation of the nematic-smectic (NS) and nematic-columnar (NC) bifurcation density with ionic strength κD for a) parallel charged rods with aspect ratio $L/D = 50$ and (b) parallel disks with surface charge patterns indicated in Fig. 1 ($D/L = 10$, $Z^2 \lambda_B / D = 10$). Solid curves indicate Nematic-Smectic (NS) bifurcations, dotted curves indicate Nematic-Columnar (NC) instabilities.

$k_C \{0, 1, 0\}$, $\mathbf{k}_2 = k_C \{\frac{\sqrt{3}}{2}, \frac{1}{2}, 0\}$, and $\mathbf{k}_3 = k_C \{-\frac{\sqrt{3}}{2}, \frac{1}{2}, 0\}$ describing a two-dimensional triangular lattice perpendicular to the director.

The results in Fig. 6 reveal a marked stabilization of columnar with respect to smectic order for rodlike cylinders at low ionic strength. This outcome is in accordance with previous numerical results for Yukawa rods in a strong external aligning field [52]. Needless to say that the transition values are merely qualitative and that the volume fractions can be brought down to more realistic values, for instance, by using an effective second-virial theory based on a resummation of higher virial coefficient (e.g. using Parsons' theory [56]). For hard parallel disks, the nematic-smectic always pre-empts the nematic-columnar one irrespective of the aspect ratio x . This implies that the parallel approximation fares rather badly for hard discotic systems which are known to form columnar phases only [9, 95]. Nevertheless some general trends for can be gleaned from Fig. 6b such as an apparently stabilization of smectic order for uniformly charged disks in the low screening regime. The prevalence of smectic order has been recently reported in weakly screened discotic systems [96]. As for the other charge patterns, the observation from Fig. 6 that both smectic and columnar-type order are destabilized upon reducing the screening could hint at more complicated instability mechanisms

prevailing in the low screening region, such as those pertaining to crystalline order where both longitudinal and transverse density modulations compete with spatial inhomogeneities in the director field [45].

We wish to emphasize that the approach outlined above is generic in that it provides a simple route to gauge the effect of soft interactions on the stability of positionally ordered liquid crystals. It can be applied to a vast range of model systems with various segment potentials (provided integrable) and form factors. Instabilities from nematic to other liquid crystals symmetries or three-dimensional crystals (e.g. fcc or bcc) can easily be included by adapting the \mathbf{k} vectors to the desired Bravais lattice. In order to describe fully crystalline states we may exploit the fact that particles are strongly localized around their lattice site to construct an appropriate density functional representation for the excess Helmholtz free energy. In the following, we shall briefly sketch the approach outlined in Refs. [97, 98]. The central assumption is that the density profile of the solid consists of Gaussian peaks centred on a predefined lattice vector $\{\mathbf{R}_i\}$ factorized with the orientational probability (ODF) $f(\Omega)$. If we assume a spatially homogeneous director field, the one-body density can be written as:

$$\rho(\mathbf{r}, \Omega) = f(\Omega) \sum_{i=1}^N G(\mathbf{r} - \mathbf{R}_i), \quad (43)$$

with

$$G(\mathbf{r} - \mathbf{R}_i) = \left(\frac{\alpha}{\pi}\right)^{3/2} \exp[-\alpha(\mathbf{r} - \mathbf{R}_i)^2], \quad (44)$$

where α is a parameter which describes how localised the particles are around each lattice site. Assuming the proportion of lattice defects to be negligible, each lattice site should contain only one particle as reflected in the normalisation of Eq. (44). The excess free energy of the system can be expressed in terms of the following Fourier integral:

$$F_{\text{ex}} = -\frac{k_B T}{2} \sum_{i \neq j} \frac{1}{(2\pi)^3} \int d\mathbf{k} e^{i\mathbf{k} \cdot \mathbf{R}_{ij}} \hat{G}(k)^2 \langle \langle \hat{\Phi}(\mathbf{k}; \Omega, \Omega') \rangle \rangle, \quad (45)$$

which is composed of the FT of the orientation-dependent Mayer kernel Eq. (41), and the Gaussian weight $\hat{G}(k) = \exp(-k^2/4\alpha)$. In general, the radially symmetric form Eq. (44) is justified only if particles are strongly localized around their lattice points ($\alpha \gg 1$) so that the density peaks are not affected by the symmetry of the underlying lattice. The total free energy is obtained by combining the excess free energy with the ideal free energy associated with the Gaussian parameterization:

$$F_{\text{id}} = N k_B T \left\{ \frac{3}{2} \ln \left(\frac{\nu^2 \alpha}{\pi} \right) - \frac{5}{2} + \langle \ln f(\Omega) \rangle \right\}. \quad (46)$$

Next, the free energy must be minimized with respect to the localization parameter α , the set of relevant lattice

constants corresponding to the imposed lattice symmetry [99] and $f(\Omega)$. This simple variational scheme allows one to compare the stability of various crystal symmetries as a function of density and interaction range and strength. In addition, due to the translation-orientation coupling via f , both aligned and rotationally disordered plastic crystal states can be included. Phase transitions between fluid and crystal phases can be probed by equating the pressure and chemical potential emerging from the Gaussian free energy with those of the fluid phases, Eq. (17).

VI. CONCLUDING REMARKS

We have proposed a generalized Onsager theory for strongly non-spherical colloidal particles with an intrinsic patchiness in the interaction potential. The theory supplements the second-virial reference free energy for the hard-core interaction with a first-order perturbative (van der Waals) term, which captures the directional soft interactions between the rods or the disks. As such, the theory interpolates between the low density regime, where the second-virial approximation holds, and the high density regime where the mean-field approach is accurate. We have aimed at formulating a generic framework that should be applicable to a wide range of particle shapes, ranging from elongated rods to flat, sheet-like disks with an arbitrary spatial organization of interactions sites distributed along the colloid surface. By recasting the mean-field contribution in terms a Fourier series, the excess free energy naturally factorizes into three main contributions: the site-site interaction potential, the shape of the colloidal hard-core, and a form factor associated with the spatial arrangement of the interaction site residing on each particle.

As a test case, we have applied our theory to investigate orientation disorder-order transitions in fluids of charged rods and disks with a uniform, localized or discretized surface charge pattern. The results for the isotropic-nematic phase diagram and the instability analysis of transverse and longitudinal freezing of a nematic fluid in the high-density regime, reveal a picture that is consistent with results from more elaborate Poisson-Boltzmann approaches and particle simulation. This lends credence to our theory as a practical tool to assess the influence of soft patchy interactions on the liquid crystal phase diagram of non-isometric colloids. Although the focus of this study is on the liquid crystal fluid phases that emerge at relatively low particle density, the stability of spatially ordered liquid crystals at higher particle concentration can also be scrutinized using a simple bifurcation analysis while fully crystalline phases can be expediently accounted for using a Gaussian parameterization for the one-body density often used in density functional theories of freezing.

We remark that the present theory is amenable to various extensions towards more complicated systems. Col-

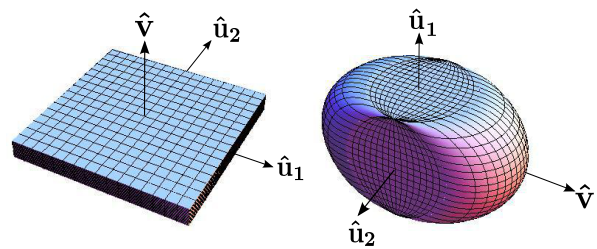


FIG. 7: The excluded-volume manifold of two infinitely slender cylindrical rods ($L/D \rightarrow \infty$) is a parallelepiped spanned by the particle-based coordinate frame $\{\hat{\mathbf{u}}_1, \hat{\mathbf{u}}_2, \hat{\mathbf{v}}\}$ (left figure) whereas that of two infinitely thin disks ($L/D \downarrow 0$) is represented by a sphero-cuboid (right figure). Both manifolds correspond to the case where the cylinders are perpendicular to each other ($\hat{\mathbf{u}}_1 \perp \hat{\mathbf{u}}_2$).

loidal dispersions composed of non-spherical particles are rarely monodisperse but are often characterized by a continuous spread in particle sizes. The polydisperse nature of the colloid shape and/or the amplitude of the soft interactions can be incorporated in a straightforward manner [100, 101]. Bio-colloids such as stiff viral rods [102] and DNA are commonly characterized by an intrinsic helical patchiness which has profound implications on the mesostructure in bulk and confinement [103]. The present theory could be extended to relate the mesoscopic chirality of twisted nematics to the intrinsic helical form factor of the colloid [104].

Last but not least, similar to systems of spherical subunits [105, 106], more accurate reference free energies could be employed which should give a more reliable account of correlations in systems of less anisometric colloids (dumbbells, thick platelets, polyhedra), which routinely form highly ordered (liquid) crystals at high particle volume fraction [107, 108].

Appendix: excluded volume of strongly anisometric cylinders

In this Appendix, we derive expressions for the Fourier Transform (FT) of the excluded volume manifold of two infinitely slender rods and disks, featured in Eq. (12) of the main text. The excluded volume of two hard cylinders at fixed angle γ is a *parallelepiped* which can be parameterized by switching from the laboratory frame to a particle frame spanned by the normal orientational unit vectors $\hat{\mathbf{u}}_\alpha$ of the cylinder pair. Let us define the additional unit vectors:

$$\begin{aligned} \hat{\mathbf{v}}|\sin \gamma| &= \hat{\mathbf{u}}_1 \times \hat{\mathbf{u}}_2 \\ \hat{\mathbf{w}}_\alpha &= \hat{\mathbf{u}}_\alpha \times \hat{\mathbf{v}} \quad (\alpha = 1, 2), \end{aligned} \quad (47)$$

so that $\{\hat{\mathbf{u}}_\alpha, \hat{\mathbf{v}}, \hat{\mathbf{w}}_\alpha\}$ are two orthonormal basis sets in 3D. The centre-of-mass distance vector can be uniquely

decomposed in terms of these basis vectors:

$$\mathbf{r} = (\mathbf{r} \cdot \hat{\mathbf{u}}_\alpha)\hat{\mathbf{u}}_\alpha + (\mathbf{r} \cdot \hat{\mathbf{v}})\hat{\mathbf{v}} + (\mathbf{r} \cdot \hat{\mathbf{w}}_\alpha)\hat{\mathbf{w}}_\alpha. \quad (48)$$

The leading order contribution to the excluded-volume body is of $\mathcal{O}(L^2D)$ and stems from the overlap of the cylindrical parts of the cylinders. This resulting parallelepiped can be parameterized as follows:

$$\mathbf{r}_{cc} = \frac{L}{2}t_1\hat{\mathbf{u}}_1 + \frac{L}{2}t_2\hat{\mathbf{u}}_2 + Dt_3\hat{\mathbf{v}}, \quad (49)$$

with $-1 \leq t_i \leq 1$ for $i = 1, 2, 3$. The Jacobian associated with the coordinate transformation is $J_{cc} = \frac{1}{4}L^2D|\sin \gamma|$. The FT of the parallelepiped is thus given by:

$$\begin{aligned} \hat{v}_{\text{excl}}(\Omega_1, \Omega_2) &= \int d\mathbf{r}_{cc} e^{i\mathbf{q} \cdot \mathbf{r}_{cc}} \\ &= J_{cc} \prod_{i<3} \int_{-1}^1 dt_i \cos(\mathbf{q} \cdot \mathbf{r}_{cc}) \\ &= v_0 |\sin \gamma| \mathcal{F}(\mathbf{q}; \Omega_1, \Omega_2), \end{aligned} \quad (50)$$

where $v_0 = 2L^2D$. Using that $\int_{-1}^1 dx \cos(ax + b) = 2j_0(x) \cos b$ one obtains for strongly elongated cylinders (needles):

$$\mathcal{F}(\mathbf{q}; \Omega_1, \Omega_2) = j_0\left(\frac{L}{2}\mathbf{q} \cdot \hat{\mathbf{u}}_1\right) j_0\left(\frac{L}{2}\mathbf{q} \cdot \hat{\mathbf{u}}_2\right) j_0(D\mathbf{q} \cdot \hat{\mathbf{v}}), \quad (51)$$

in terms of the spherical Bessel function $j_0(x) = \sin x/x$. A similar procedure can be carried out for disk-shaped cylinders. Two infinitely flat cylinders overlap if the separation \mathbf{r} of their centre-of-mass is in a sphero-cuboid (see Fig. 7) which can be parameterized as follows:

$$\mathbf{r}_{cc} = -\frac{D}{2}t_1\hat{\mathbf{w}}_1 - \frac{D}{2}t_2\hat{\mathbf{w}}_2 + \frac{D}{2}t_3[(1-t_1^2)^{1/2} + (1-t_2^2)^{1/2}]\hat{\mathbf{v}}, \quad (52)$$

with $-1 \leq t_i \leq 1$ for $i = 1, 2, 3$. The Jacobian associated with the transformation from the lab to the particle frame is $d\mathbf{r}_{cc} = J_{cc}dt_1d_2dt_3$ with $J_{cc} = \frac{D^3}{8}|\sin \gamma|[(1-t_1^2)^{1/2} + (1-t_2^2)^{1/2}]$. Similar to the case of rods the FT of the excluded volume figure is cast into a cosine transform according to Eq. (50) substituting $v_0 = \pi D^3/2$ for disks. The shape function \mathcal{F} , however, requires a bit more effort in this case. First, the integration over t_3 can be

carried out straightforwardly using the relation involving the spherical Bessel function mentioned above Eq. (51). This yields:

$$\begin{aligned} \mathcal{F} &= \frac{1}{\pi D\mathbf{q} \cdot \hat{\mathbf{v}}} \int_{-1}^1 dt_1 \int_{-1}^1 dt_2 \cos\left(\frac{D}{2}t_1\mathbf{q} \cdot \hat{\mathbf{w}}_1 + \frac{D}{2}t_2\mathbf{q} \cdot \hat{\mathbf{w}}_2\right) \\ &\quad \times \sin\{[(1-t_1^2)^{1/2} + (1-t_2^2)^{1/2}]\frac{D}{2}\mathbf{q} \cdot \hat{\mathbf{v}}\}. \end{aligned} \quad (53)$$

The double integral can be split into single integrals using standard trigonometric manipulations. Rearranging terms gives the final expression for infinitely flat discotic cylinders (disks):

$$\mathcal{F}(\mathbf{q}; \Omega_1, \Omega_2) = \frac{1}{\pi D\mathbf{q} \cdot \hat{\mathbf{v}}} (A_1B_2 + A_2B_1), \quad (54)$$

in terms of the orientation-dependent functions:

$$\begin{aligned} A_\alpha &= \int_{-1}^1 dt \cos\left(\frac{D}{2}t\mathbf{q} \cdot \hat{\mathbf{w}}_\alpha\right) \cos\left(\frac{D}{2}(1-t^2)^{1/2}\mathbf{q} \cdot \hat{\mathbf{v}}\right) \\ B_\alpha &= \int_{-1}^1 dt \cos\left(\frac{D}{2}t\mathbf{q} \cdot \hat{\mathbf{w}}_\alpha\right) \sin\left(\frac{D}{2}(1-t^2)^{1/2}\mathbf{q} \cdot \hat{\mathbf{v}}\right) \end{aligned} \quad (55)$$

The last integral can be solved in closed form by substituting $t = \cos \theta$ and invoking Catalan's integral representation of Bessel functions [109]:

$$J_0(\sqrt{\beta^2 - \alpha^2}) = \frac{1}{\pi} \int_0^\pi d\theta e^{\alpha \cos \theta} \cos(\beta \sin \theta), \quad (56)$$

with $J_n(x)$ a Bessel function of the first kind. With this, the solution of Eq. (55) can be found by taking the partial derivative to α on both sides and rearranging terms:

$$B_\alpha = \frac{\pi}{2} (\mathbf{q} \cdot \hat{\mathbf{v}}) J_1(\tilde{q}_\alpha) / (\tilde{q}_\alpha), \quad (57)$$

where $\tilde{q}_\alpha = [(\frac{D}{2}\mathbf{q} \cdot \hat{\mathbf{w}}_\alpha)^2 + (\frac{D}{2}\mathbf{q} \cdot \hat{\mathbf{v}})^2]^{1/2}$. Despite the similarity between A and B there is no closed analytical expression available for A but the one-dimensional integral is readily evaluated using standard numerical integration routines.

[1] P. G. de Gennes and J. Prost, *The Physics of Liquid Crystals* (Clarendon Press, Oxford, 1993).
[2] L. Onsager, Ann. N.Y. Acad. Sci. **51**, 627 (1949).
[3] M. P. Taylor, R. Hentschke, and J. Herzfeld, Phys. Rev. Lett. **62**, 800 (1989).
[4] P. Bolhuis and D. Frenkel, J. Chem. Phys. **106**, 666 (1997).
[5] S. C. McGrother, D. C. Williamson, and G. Jackson, J. Chem. Phys. **104**, 6755 (1996).

[6] A. M. Bohle, R. Holyst, and T. Vilgis, Phys. Rev. Lett. **76**, 1396 (1996).
[7] H. Graf and H. Löwen, Phys. Rev. E **59**, 1932 (1999).
[8] H. Graf and H. Löwen, J. Phys.; Condens. Matter **11**, 1435 (1999).
[9] J. A. C. Veerman and D. Frenkel, Phys. Rev. A **45**, 5632 (1992).
[10] H. H. Wensink and H. N. W. Lekkerkerker, Mol. Phys. **107**, 2111 (2009).

- [11] M. Marechal, A. Cuetos, B. Martínez-Haya, and M. Dijkstra, *J. Chem. Phys.* **134**, 094501 (2011).
- [12] D. Frenkel, H. N. W. Lekkerkerker, and A. Stroobants, *Nature* **332**, 822 (1988).
- [13] D. Frenkel, *Liq. Cryst.* **5**, 929 (1989).
- [14] E. Verwey and J. Overbeek, *Theory of the Stability of Lyophobic Colloids* (Elsevier, Amsterdam, 1948).
- [15] J.-P. Hansen and H. Löwen, *Annu. Rev. Phys. Chem.* **51**, 209 (2000).
- [16] A. Vrij, *Pure Appl. Chem.* **48**, 471 (1976).
- [17] H. N. W. Lekkerkerker and R. Tuinier, *Colloids and the Depletion Interaction*, Lecture Notes in Physics (Springer, 2011).
- [18] T. Kato, in *Molecular Self-Assembly Organic Versus Inorganic Approaches*, edited by M. Fuiita (Springer Berlin Heidelberg, 2000), vol. 96 of *Structure and Bonding*, pp. 95–146.
- [19] N. Geerts and E. Eiser, *Soft Matter* **6**, 4647 (2010).
- [20] S. McGrother, R. Sear, and G. Jackson, *J. Chem. Phys.* **106**, 7315 (1997).
- [21] C. De Michele, T. Bellini, and F. Sciortino, *Macromolecules* **45**, 1090 (2012).
- [22] C. Avendaño, A. Gil-Villegas, and E. González-Tovar, *Chem. Phys. Lett.* **470**, 67 (2009).
- [23] A. A. Shah, B. Schultz, K. L. Kohlstedt, S. C. Glotzer, and M. J. Solomon, *Langmuir* **29**, 4688 (2013).
- [24] X. Ye, J. Chen, M. Engel, J. A. Millan, W. Li, L. Qi, G. Xing, J. E. Collins, C. R. Kagan, J. Li, et al., *Nature Chemistry* **5**, 466 (2013).
- [25] S. C. Glotzer and M. J. Solomon, *Nature Materials* **6**, 557 (2007).
- [26] M. A. Cotter, *J. Chem. Phys.* **66**, 4710 (1977).
- [27] M. A. Cotter, in *The molecular physics of liquid crystals*, edited by G. R. Luckhurst and G. W. Gray (Academic Press, New York, 1979).
- [28] W. M. Gelbart and B. A. Baron, *J. Chem. Phys.* **66**, 207 (1977).
- [29] S. Varga and G. Jackson, *Mol. Phys.* **104**, 3681 (2006).
- [30] M. Franco-Melgar, A. J. Haslam, and G. Jackson, *Mol. Phys.* **106**, 649 (2008).
- [31] W. Maier and A. Saupe, *Z. Naturforsch.* **13a**, 564 (1959); *ibid.* **14a**, 882 (1959); *ibid.* **15a**, 287 (1960).
- [32] G. R. Luckhurst and C. Zannoni, *Nature* **267**, 412 (1977).
- [33] H. van Olphen, *An Introduction to Clay Colloid Chemistry* (Wiley and Sons, New York, 1963).
- [34] P. Davidson and J. C. P. Gabriel, *Curr. Opin. Colloid Interface Sci.* **9**, 377 (2005).
- [35] B. J. Lemaire, P. Davidson, J. Ferré, J. P. Jamet, D. Petermann, P. Panine, I. Dozov, and J. P. Jolivet, *Eur. Phys. J. E* **13**, 309 (2004).
- [36] S. Roorda, T. van Dillen, A. Polman, C. Graf, A. van Blaaderen, and B. Kooi, *Adv. Mater.* **16**, 235 (2004).
- [37] Z. Zhang and J. van Duijneveldt, *J. Chem. Phys.* **124**, 154910 (2006).
- [38] A. Mourchid, A. Delville, J. Lambard, E. Lecolier, and P. Levitz, *Langmuir* **11**, 1942 (1995).
- [39] B. Ruzicka, E. Zaccarelli, L. Zulian, R. Angelini, M. Sztucki, A. Moussaid, T. Narayanan, and F. Sciortino, *Nature Materials* **10**, 56 (2011).
- [40] G. C. Ganzenmüller and G. N. Patey, *Phys. Rev. Lett.* **105**, 137801 (2010).
- [41] E. Trizac, L. Bocquet, R. Agra, J. Weis, and M. Aubouy, *J. Phys.; Condens. Matter* **14**, 9339 (2002).
- [42] L. Morales-Anda, H. H. Wensink, A. Galindo, and A. Gil-Villegas, *J. Chem. Phys.* **136**, 034901 (2012).
- [43] M. Delhomme, C. Labbez, and B. Jönsson, *J. Phys. Chem. Lett.* **3**, 1315 (2012).
- [44] J. de Graaf, N. Boon, M. Dijkstra, and R. van Roij, *J. Chem. Phys.* **137**, 104910 (2012).
- [45] S. Jabbari-Farouji, J.-J. Weis, P. Davidson, P. Levitz, and E. Trizac (2013), preprint, arxiv.org/abs/1212.5043.
- [46] M. Delhomme, B. Jönsson, and C. Labbez, *Soft Matter* **8**, 9691 (2012).
- [47] G. Odriozola, M. Romero-Bastida, and F. de J. Guevara-Rodríguez, *Phys. Rev. E* **70**, 021405 (2004).
- [48] S. Kutter, J.-P. Hansen, M. Sprik, and E. Boek, *J. Chem. Phys.* **112**, 311 (2000).
- [49] D. Léger and D. Levesque, *J. Chem. Phys.* **116**, 2251 (2002).
- [50] A. Walther and A. H. E. Mueller, *Soft Matter* **4**, 663 (2008).
- [51] L. Cheng, G. Zhang, L. Zhu, D. Chen, and M. Jiang, *Angew. Chem. Int. Ed.* **47**, 10171 (2008).
- [52] H. H. Wensink, *J. Chem. Phys.* **126**, 194901 (2007).
- [53] H. Hansen-Goos and K. Mecke, *Phys. Rev. Lett.* **102**, 018302 (2009).
- [54] H. Hansen-Goos and J. S. Wettlaufer, *J. Chem. Phys.* **134**, 014506 (2011).
- [55] J. Cuesta and Y. Martínez-Ratón, *J. Chem. Phys.* **107**, 6379 (1997).
- [56] J. D. Parsons, *Phys. Rev. A* **19**, 1225 (1979).
- [57] Y. Rosenfeld, M. Schmidt, H. Löwen, and P. Tarazona, *Phys. Rev. E* **55**, 4245 (1997).
- [58] M. Bier, L. Harnau, and S. Dietrich, *J. Chem. Phys.* **125**, 184704 (2006).
- [59] D. Costa, J.-P. Hansen, and L. Harnau, *Mol. Phys.* **103**, 1917 (2005).
- [60] L. Harnau, *Mol. Phys.* **106**, 1975 (2008).
- [61] S. Kondrat, M. Bier, and L. Harnau, *J. Chem. Phys.* **132**, 184901 (2010).
- [62] C. Likos, *Phys. Rep.* **348**, 267 (2001).
- [63] E. Eggen, M. Dijkstra, and R. van Roij, *Phys. Rev. E* **79**, 041401 (2009).
- [64] J. N. Israelachvili, *Intermolecular and surface forces* (Academic Press, London, 1991).
- [65] B. J. Berne and P. Pechukas, *J. Chem. Phys.* **56**, 4213 (1972).
- [66] C. N. Likos, *Soft Matter* **2**, 478 (2006).
- [67] P. Bolhuis, A. Stroobants, D. Frenkel, and H. Lekkerkerker, *J. Chem. Phys.* **107**, 1551 (1997).
- [68] E. del Rio, A. Galindo, and E. de Miguel, *Phys. Rev. E* **72**, 051707 (2005).
- [69] L. Lue, *Fluid Phase Equil.* **241**, 236 (2006).
- [70] M. M. Hatlo, P. Banerjee, J. Forsman, and L. Lue, *J. Chem. Phys.* **137**, 064115 (2012).
- [71] J. Herzfeld, A. E. Berger, and J. W. Wingate, *Macromolecules* **17**, 1718 (1984).
- [72] S. Alexander, P. M. Chaikin, P. Grant, G. J. Morales, P. Pincus, and D. Hone, *J. Chem. Phys.* **80**, 5776 (1984).
- [73] M. Deserno and C. Holm, in *Electrostatic Effects in Soft Matter and Biophysics*, edited by C. Holm, P. Kekicheff, and R. Podgornik (2001), vol. 46 of *Nato Science Series II: Mathematics, Physics and Chemistry*, pp. 27–50.
- [74] E. Trizac and Y. Levin, *Phys. Rev. E* **69**, 031403 (2004).
- [75] J. Dobnikar, R. Castañeda-Priego, H. H. von Grünberg,

- and E. Trizac, *New J. Phys.* **8**, 277 (2006).
- [76] Y. Levin, E. Trizac, and L. Bocquet, *J. Phys.; Condens. Matter* **15**, S3523 (2003).
- [77] E. Trizac, L. Belloni, J. Dobnikar, H. H. von Grünberg, and R. Castañeda-Priego, *Phys. Rev. E* **75**, 011401 (2007).
- [78] B. Zoetekouw and R. van Roij, *Phys. Rev. E* **73**, 021403 (2006).
- [79] M. Askari and J. Abouie, *J. Phys.; Condens. Matter* **23**, 155103 (2011).
- [80] D. Chapot, L. Bocquet, and E. Trizac, *J. Chem. Phys.* **120**, 3969 (2004).
- [81] D. Chapot, L. Bocquet, and E. Trizac, *J. Colloid Interface Sci.* **285**, 609 (2005).
- [82] A. Stroobants, H. N. W. Lekkerkerker, and T. Odijk, *Macromolecules* **19**, 2232 (1986).
- [83] M. Fixman and J. Skolnick, *Macromolecules* **11**, 863 (1978).
- [84] J. Schneider, W. Hess, and R. Klein, *J. Phys. A: Math. Gen.* **18**, 1221 (1984).
- [85] J. Deutsch and N. Goldenfeld, *J. Physique* **43**, 651 (1982).
- [86] R. Agra, E. Trizac, and L. Bocquet, *Eur. Phys. J. E* **15**, 345 (2004).
- [87] C. Álvarez and G. Téllez, *J. Chem. Phys.* **133**, 144908 (2010).
- [88] E. Trizac, M. Aubouy, and L. Bocquet, *J. Phys.; Condens. Matter* **15**, S291 (2003).
- [89] T. Sokolovska, M. Cates, and R. Sokolovskii, *Phys. Rev. Lett.* **90**, 235701 (2003).
- [90] M. P. Allen, G. T. Evans, D. Frenkel, and B. M. Mulder, *Adv. Chem. Phys.* **86**, 1 (1993).
- [91] Y. Singh, *Phys. Rep.* **207**, 351 (1991).
- [92] R. F. Kayser and H. J. Raveché, *Phys. Rev. A* **17**, 2067 (1978).
- [93] B. M. Mulder, *Phys. Rev. A* **35**, 3095 (1987).
- [94] R. van Roij, P. Bolhuis, B. Mulder, and D. Frenkel, *Phys. Rev. E* **52**, 1277 (1995).
- [95] F. M. van der Kooij and H. N. W. Lekkerkerker, *J. Phys. Chem. B* **102**, 7829 (1998).
- [96] D. Kleshchanok, P. Holmqvist, J.-M. Meijer, and H. N. W. Lekkerkerker, *J. Am. Chem. Soc.* **134**, 5985 (2012).
- [97] H. Xu, H. N. W. Lekkerkerker, and M. Baus, *Europhys. Lett.* **17**, 163 (1992).
- [98] A. Archer, *Phys. Rev. E* **72**, 051501 (2005).
- [99] M. Baus, *Mol. Phys.* **50**, 543 (1983).
- [100] M. Baus, L. Bellier-Castella, and H. Xu, *J. Phys.; Condens. Matter* **14**, 9255 (2002).
- [101] H. H. Wensink and G. J. Vroege, *J. Chem. Phys.* **119**, 6868 (2003).
- [102] E. Grelet and S. Fraden, *Phys. Rev. Lett.* **90**, 198302 (2003).
- [103] A. Leforestier, A. Berlin, J. Dubochet, K. Richter, N. S. Blanc, and F. Livolant, *C. R. Chimie* **11**, 229 (2008).
- [104] H. H. Wensink and G. Jackson, *J. Phys.; Condens. Matter* **23**, 194107 (2011).
- [105] A. Malijevský, P. Bryk, and S. Sokolowski, *Phys. Rev. E* **72**, 032801 (2005).
- [106] R. Roth, *Mol. Phys.* **109**, 2897 (2011).
- [107] C. Vega, E. Paras, and P. Monson, *J. Chem. Phys.* **96**, 9060 (1992).
- [108] P. F. Damasceno, M. Engel, and S. C. Glotzer, *Science* **337**, 453 (2012).
- [109] H. Bateman and A. Erdélyi, *Tables of Integral Transforms*, vol. 1 (McGraw-Hill, 1954).
- [110] This form represents a simplified subset of more general orientation-dependent segment potentials of the form $u(\mathbf{r}; \Omega_1^{(l)}, \Omega_2^{(m)})$, such as for e.g. segment dipoles, where u depends on the orientation $\Omega_1^{(l)}$ of site vector l with respect to the molecular frame of particle 1.